AGU PUBLICATIONS

Water Resources Research

RESEARCH ARTICLE
10.1002/2017WR020768

Generation of complex karstic conduit networks with a hydrochemical model

Rob de Rooij[1] and Wendy Graham[1]

[1]Water Institute, University of Florida, Gainesville, Florida, USA

Key Points:
- A speleogenesis model is presented that can be used to generate conduit networks at a regional scale
- Our model accounts for a switch between hydraulic and catchment control and uses an implicit reactive-transport scheme
- The model is applied to a real system and it is illustrated that the model can generate a realistic conduit network

Correspondence to:
R. de Rooij,
r.derooij@ufl.edu

Citation:
de Rooij, R., and W. Graham (2017), Generation of complex karstic conduit networks with a hydrochemical model, *Water Resour. Res.*, *53*, 6993–7011, doi:10.1002/2017WR020768.

Received 14 MAR 2017
Accepted 18 JUL 2017
Accepted article online 24 JUL 2017
Published online 17 AUG 2017

Abstract In this paper, we present a hydrochemical model that can be used to generate plausible karstic conduit networks that honor what is known about geology, hydrology, and topography of a karst system. To make the model applicable to a range of natural karst systems, we introduce a flexible and physically realistic flow boundary condition along the land surface. Moreover, whereas comparable existing speleogenesis models use an explicit reactive-transport scheme, we propose an implicit reactive-transport scheme to permit a coarser spatial discretization of the conduit cells. An application to a real karst system illustrates that the model can generate a realistic karstic network that reproduces observed hydrologic behavior in terms of current spring flow rates, regional hydraulic head field as well as average groundwater residence times. Our model provides a useful tool to generate ensembles of possible karstic conduit networks that may be used within a stochastic framework to analyze flow and transport prediction uncertainty associated with a lack of knowledge about network geometry.

1. Introduction

A typical characteristic of a karst aquifer is the presence of a hierarchical conduit network. This network is formed by a positive feedback mechanism between dissolution by water undersaturated with respect to calcite and the amount of water percolating through a carbonate rock [*Palmer*, 1991]. Namely, as conduits grow due to dissolution, more undersaturated water can flow through the conduits enhancing the rate of dissolution. Due to this mechanism, larger conduits grow faster at the expense of smaller ones and hierarchical networks form. Concurrently with conduit development, sinkholes and swallets form focusing recharge into the conduit network [*Palmer*, 1991]. Discharge also becomes more focused at karst springs during karst evolution. Conduits are characterized by relatively low groundwater storage and relatively high groundwater flow velocities compared to the surrounding fractured carbonate rock matrix [*Kaufmann*, 2003]. In evolved karst aquifers, conduit flow is typically turbulent.

Given the internal structure and hydrodynamic functioning of karst aquifers, the discrete-continuum modeling approach, in which karstic conduits are explicitly represented as discrete one-dimensional features embedded in a porous rock continuum, is well suited to simulate flow and solute transport processes in karst aquifers [*de Rooij et al.*, 2013; *Kiraly*, 1985, 1998; *Shoemaker et al.*, 2008]. However, since generally little is known about the conduit network, the application of discrete-continuum models as a management or prediction tool has remained limited. Instead, discrete-continuum models have most often been used as learning tools. Assuming a hypothetical and a relatively simple conduit network geometry, these models have been used for testing classical methods of spring hydrograph analysis [*Eisenlohr et al.*, 1997a, 1997b], to examine spring responses [*Birk et al.*, 2006], and to gain insights into the hydrodynamic functioning of the epikarst [*Eisenlohr et al.*, 1997a; *Kiraly et al.*, 1995], the effects of turbulent flow in the conduits [*Reimann et al.*, 2011], and the effects of exchange flow between the conduits and the matrix [*Hill et al.*, 2010] and speleogenesis processes [*Bauer et al.*, 2003, 2005; *Kaufmann*, 2003]. Discrete-continuum models have been applied to real karst systems [*Gallegos et al.*, 2013; *Kovacs and Jeannin*, 2003; *Xu et al.*, 2015], but within these applications the uncertainty with respect to the conduit network is not considered.

Stochastic approaches have been used to gain insights into the relation between network geometry and solute transport for hypothetical karst systems [*Borghi et al.*, 2016; *Ronayne*, 2013]. A stochastic approach requires efficient means of generating ensembles of possible conduit network realizations. Several

approaches exist to generate such ensembles. Structure imitating approaches aim to reproduce the structure of the conduit network by purely statistical means. The approach of *Pardo-Iguzquiza et al*. [2012] is based on resampling from templates to generate individual conduit segments and a diffusion-limited aggregation method to generate the connectivity between the segments. *Ronayne* [2013] proposed a nonlooping invasion percolation model as proposed by *Stark* [1991] to generate conduit networks. An overall problem of the structure imitating approach is that it remains an unresolved challenge how to generate realistic connectivity patterns by purely statistical means. The diffusion-limited aggregation method of *Pardo-Iguzquiza et al*. [2012] forces connections between the conduits and the resulting connectivity is not governed by statistical input parameters. The nonlooping invasion percolation model as used by *Ronayne* [2013] defines a priori a network without loops, a connectivity pattern more typical for stream networks than for conduit networks. New insights into how to describe conduit connectivity patterns in terms of statistical characteristics [*Collon et al*., 2017; *Hendrick and Renard*, 2016] may ultimately lead to improved methods to generate realistic connectivity patterns by purely statistical means.

Alternatively, conduit networks may be generated by a process-imitating approach. This approach is based on mimicking the speleogenesis process underlying the formation of conduits. This approach accounts for the self-organizing nature of the conduit network due to the positive feedback mechanism between dissolution and flow. As such this approach has good potential to generate realistic connectivity patterns. Typically, process-imitating approaches are not based on speleogenesis models. Instead, the positive feedback mechanism is simulated by an iterative process in which conduits are progressively widened using a heuristic erosion potential. By defining a heuristic erosion potential, the simulation of reactive-solute transport (as necessary in a speleogenesis model) is avoided and the modeling is simplified. The approach proposed by *Jaquet et al*. [2004] is based on a modified lattice-gas automaton in which walkers with a certain erosion potential travel through the medium. *Borghi et al*. [2012] use a pseudo-genetic approach in which conduits are eroded along minimum effort pathways as computed by a fast-marching algorithm. In the methodology of *Lafare* [2012], conduits are generated using a heuristic erosion potential function depending on the flow velocities and water ages.

To date, speleogenesis models have not been used as an efficient approach to generate realistic conduit networks, but rather to gain insights into the evolution of the conduits in hypothetical and highly schematized karst systems [*Dreybrodt et al*., 2010; *Gabrovsek and Dreybrodt*, 2010; *Kaufmann*, 2003, 2009; *Kaufmann et al*., 2010]. However, since speleogenesis models simulate the positive feedback mechanism between dissolution and flow, they have good potential to generate realistic conduit networks.

The reconstruction of hydrological conditions during the conduit formation process poses a significant problem when applying process-imitating approaches. Namely, the resulting conduit network may depend critically on the applied flow boundary conditions. Therefore, it is important to recognize that as the drainage capacity of the conduit network increases, a karst system will switch from hydraulic to catchment control, as pointed out by *Palmer* [1991]. As discussed by *Bauer et al*. [2005], incorporating this switch into a speleogenesis model by using time-variant recharge conditions permits more physically realistic flow boundary conditions during karst genesis modeling. During the early stages of karst evolution, the subsurface cannot accommodate the available recharge as subsurface flow is limited by the subsurface drainage capacity. During this time, the karst system is under hydraulic control and the system can be driven by a fixed head boundary along the land surface [*Bauer et al*., 2005]. As subsurface drainage capacity increases due to the development of the conduit network, the subsurface can eventually drain all the available recharge. At this stage, the karst system is under catchment control and this stage may be simulated by applying a recharge flux boundary condition to the subsurface. In the work of *Bauer et al*. [2005], the switch from hydraulic to catchment control is governed by user-defined threshold conditions. A global switch is performed if the total amount of water recharging the conduit network is greater than a user-defined fraction of the total available recharge. User-defined maximum flow rates at the entrances of the conduit network are used to perform local switches from hydraulic to catchment control. Although *Bauer et al*. [2005] clearly illustrate the importance of the feedback between recharge conditions and conduit evolution, their switch algorithm depends on threshold conditions which are difficult to quantify.

In this study, we propose a speleogenesis model to generate realistic karstic networks. Although our model shares many aspects with existing speleogenesis models, we propose a few advances. Existing speleogenesis models typically require a fine conduit discretization to avoid numerical saturation with respect to calcite

when solving the reactive-transport problem [*Dreybrodt*, 1996]. We propose an alternative numerical scheme to solve the reactive-transport problem that avoids this numerical saturation and allows for coarser conduit cells. We also propose an innovative physics-based boundary condition switching approach that permits a transition from hydraulic to catchment control that depends on the topography and not on user-defined threshold conditions.

This paper presents the conceptual and numerical model underlying the speleogenesis model we propose to generate realistic karstic networks and illustrates its application to a karst region in Florida, USA. In future work, we will use the model to generate ensembles of conduit networks within a global sensitivity and uncertainty analysis framework to identify sensitive model parameters that govern the evolution of the conduit network and to provide probability distributions of flow and transport predictions. Such an approach may enhance the applicability of discrete-continuum models for management and decision-making purposes.

2. Methods

2.1. Preliminaries

A speleogenesis model simulates the positive feedback loop between dissolution by water undersaturated with respect to calcite and the amount of water percolating through the carbonate rock. Each time after the model computes increased cross-sectional areas for the conduits due to dissolution at the conduit walls, the model simulates an updated flow field. Typically, a speleogenesis model must be initiated with an initial proto-conduit network with very small cross-sectional areas [*Dreybrodt*, 1996; *Kaufmann*, 2003]. In this study, we consider speleogenesis in limestone rocks.

For numerical efficiency, speleogenesis models often use a quasi-steady state approximation. Following this approximation, it is assumed that the speleogenesis process can be simulated by a sequence of steady state flow and steady state reactive-transport computations. After each steady state reactive-transport computation, the dissolution rates are applied for a specified period of time and subsequently the next steady state flow field is computed. It has been shown that the quasi-steady state approximation is a reasonable assumption when simulating the dissolution of rock minerals over geologically significant timescales [*Hanna and Rajaram*, 1998; *Lichtner*, 1988; *Ortoleva et al*., 1987]. Namely, since the density of carbonate rocks is much larger than the maximum concentration of calcite in the percolating waters, the rate of change in cross-sectional area is much slower than the rate of change in calcite concentration and the rate of change in the flow field.

Most speleogenesis models represent conduits as one-dimensional features with either circular [*Kaufmann et al*., 2010; *Liedl et al*., 2003] or rectangular [*Gabrovsek and Dreybrodt*, 2001] cross-sectional areas. Some of these models account for conduit and matrix flow [*Bauer et al*., 2003; *Kaufmann et al*., 2010; *Liedl et al*., 2003], whereas others only account for conduit flow [*Siemers and Dreybrodt*, 1998]. Other models simulate the speleogenesis process within two-dimensional fractures [*Hanna and Rajaram*, 1998; *Szymczak and Ladd*, 2009]. Our speleogenesis model is built upon the existing discrete-continuum finite difference flow model code DisCo [*de Rooij et al*., 2013]. In this model, conduits have a circular cross-sectional area and are represented as one-dimensional features embedded within a three-dimensional porous matrix. Conduits are represented by a network of interconnected one-dimensional cells and a rectilinear grid is used to discretize the matrix domain. As discussed by *de Rooij et al*. [2013], the orientation of the conduit cells is not restricted by the geometry of the rectilinear matrix grid. As such the model can handle complex conduit networks.

In this study, we assume phreatic (i.e., fully saturated) conduits. This common assumption avoids computational difficulties in simulating transitions between open and closed conduit flow and between open conduit flow and no conduit flow. Moreover, this assumption simplifies the simulation of dissolution as it acts along the entire perimeter of the conduits such that the conduits remain circular. Although speleogenesis models exist that account for a change in topography due to erosion and dissolution of carbonate rocks at the land surface [*Kaufmann*, 2009], for simplicity we assume that the topography remains constant.

2.2. Initial Conduit Network

As mentioned in the previous section, a speleogenesis model requires an initial network of proto-conduits with small cross-sectional areas. Since these conduits have a small cross-sectional area, they have a

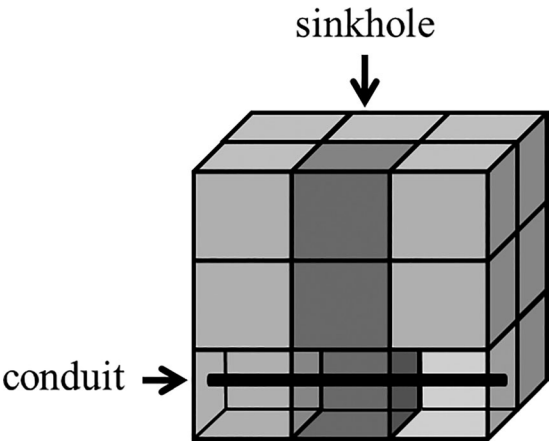

Figure 1. Representation of vertical preferential path ways by means of a stack of matrix cells with a relatively high hydraulic conductivity (dark grey).

negligible effect of the flow fields in the early stages of karst evolution. According to the inception horizon hypothesis, phreatic conduits tend to develop along inception horizons that coincide with certain bedding planes that are particularly susceptible to karstification [*Filipponi et al.*, 2010]. Moreover, fractures may control the orientation of the conduits within these bedding planes, i.e., conduits tend to form along the intersections between inception horizons and fracture planes [*Filipponi et al.*, 2010].

Two-dimensional fracture planes may be generated stochastically [*Xu and Dowd*, 2010] and inception horizons may be defined based on field evidence. However, the intersections between fracture planes and the inception horizons may not provide enough information to define a fully three-dimensional network. Consider, for example, a couple of nonintersecting bedding planes. In that case, the intersections define a network within each bedding plane, but to connect these networks, additional conduits need to be defined. To avoid this difficulty and to keep the conduit geometry relatively simple, the model presented here assumes that there is only one inception horizon. This assumption also simplifies the generation of a conduit network, since it is no longer necessary to generate fracture planes in three-dimensional space. Namely, we can directly generate a stochastic network of line segments in a two-dimensional plane and map this network onto the inception horizon. Accounting for different sets of fractures each characterized by a particular strike orientation, we define sets of line segments with corresponding strike orientations. Stochastic networks of these segments are generated using probability distribution functions to specify the location, orientation, and length of the line segments. After generating the initial conduit network, the network is mapped to the center of a subhorizontal model layer within a multilayered model domain. Since we assume fully saturated conditions in the conduits, the network must be mapped to a model layer at sufficient depth below the land surface such that the network remains below the water table during simulations.

To account for focused recharge into the conduit network, we define a number of vertical preferential flow paths that connect the conduit network with the land surface. The locations for these flow paths are generated using probability distribution functions for the conduit locations. These vertical flow paths are represented by a vertical stack of matrix cells that have a relatively high hydraulic conductivity compared to the surrounding matrix as depicted in Figure 1. Representing vertical preferential flow paths by means of vertical conduits would violate our assumption of phreatic conditions in the conduits since such vertical conduits could intersect the water table. As long as the volume occupied by these vertical stacks of matrix cells is small in comparison to the total volume of the matrix cells in those layers that contain the vertical preferential flow paths, the effect of this elevated hydraulic conductivity during the early stages of conduit evolution is minor. During later stages, as the drainage capacity of the conduit network increases, the higher hydraulic conductivity cells transmit focused recharge into the conduit network.

2.3. Calcite Dissolution

Assuming circular conduit cross sections and closed conduit flow, the change in conduit radius r [L] is given by the following mass balance at the conduit wall [*Kaufmann*, 2009]:

$$\frac{\partial r}{\partial t} = \frac{R}{\omega \rho} \tag{1}$$

where R [$M\,L^{-2}\,T^{-1}$] is the dissolution rate, t the time [T], ω is the number of moles of calcite per unit mass of calcite, and ρ is the density of calcite [$M\,L^{-3}$].

The dissolution of limestone at the conduit wall is governed by surface-controlled and transport-controlled reaction rates. The first-order surface-controlled dissolution rate R_s [$M\,L^{-2}\,T^{-1}$] is given by [*Dreybrodt*, 1988]

$$R_s = k_s\left(1 - c_s/c_{eq}\right) \tag{2}$$

where k_s is the surface-controlled rate coefficient [$M\,L^{-2}\,T^{-1}$], c_s the calcium concentration at the interface, and c_{eq} is the calcium saturation equilibrium concentration. The transport-controlled dissolution rate R_t [$M\,L^{-2}\,T^{-1}$] accounts for diffusive transport between the conduit wall and the bulk of the conduit flow and is given by [*Perne et al.*, 2014]

$$R_t = k_t(1 - c_s/c) \tag{3}$$

where k_t is the transport-controlled rate coefficient [$M\,L^{-2}\,T^{-1}$] and c the bulk calcium concentration within the water. Setting equation (2) equal to equation (3) gives an expression for c_s which can be inserted in either one of these two equations to find the following expression for the effective first-order dissolution rate R_1 [*Perne et al.*, 2014; *Szymczak and Ladd*, 2009]:

$$R_1 = k_1\left(1 - c/c_{eq}\right) \tag{4}$$

with k_1 is the effective rate coefficient [$M\,L^{-2}\,T^{-1}$]:

$$k_1 = \frac{k_t k_s}{k_t + k_s} \tag{5}$$

The transport-controlled rate coefficient k_t is given by [*Rehrl et al.*, 2008]

$$k_t = \frac{D_m N_{Sh}}{2 r c_{eq}} \tag{6}$$

where D_m is the diffusion coefficient [$L^2\,T^{-1}$] and N_{Sh} the Sherwood number. The Sherwood number for laminar conduit flow is 3.66 [*Beek and Muttzall*, 1975]. For turbulent flow, the Sherwood number may be derived using [*Beek and Muttzall*, 1975]:

$$N_{Sh} = 0.027 N_{Re}^{4/5} N_{Sc}^{1/3} \tag{7}$$

where N_{Re} and N_{sc} are the Reynolds number and the Schmidt number, respectively. The Reynolds number for conduit flow is given by

$$N_{Re} = \frac{2vr}{\upsilon} \tag{8}$$

where v is the conduit flow velocity [$L\,T^{-1}$] and υ the kinematic viscosity of water [$L^2\,T^{-1}$]. The Schmidt number is given by

$$N_{Sc} = \frac{\upsilon}{D_m} \tag{9}$$

It has been observed that as calcium concentrations approach saturation the reaction rate decreases due to impurities within the limestone which inhibit dissolution [*Svensson and Dreybrodt*, 1992]. This phenomenon known as the kinetic trigger effect [*White*, 1977] has been modeled by switching dissolution from first-order to higher order kinetics when the calcium concentration exceeds a certain value c^*. The higher order effective rate is typically given by [*Palmer*, 1991]

$$R_n = k_n\left(1 - c/c_{eq}\right)^n \tag{10}$$

where n is a value greater than one to express the higher order kinetics. To ensure that $R_1 = R_n$ at $c_b = c^*$, k_n is defined as

$$k_n = k_1\left(1 - c^*/c_{eq}\right)^{1-n} \tag{11}$$

The general expression for the reaction rate can now be written as

$$R = \begin{cases} R_1 & \text{if } c \le c^* \\ R_n & \text{if } c > c^* \end{cases} \tag{12}$$

Figure 2 illustrates the effect of the kinetic trigger on reaction rate R. The decrease in dissolution rates close to saturation allows aggressive water to penetrate further into the aquifer than would otherwise be possible.

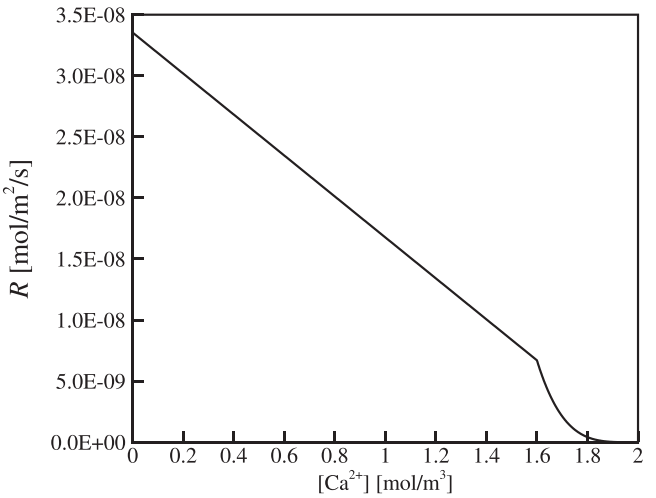

Figure 2. Reaction rate according to equation (12) with $c^* = 1.6$ mol m^{-2}.

For the parameters that appear in the equations governing calcite dissolution, we adopt the reference values from *Kaufmann* [2009]. These values are provided in Table 1.

2.4. Flow and Reactive Transport

Following the quasi-stationary state approximation, the flow and reactive-transport equations in the conduits are given by

$$\begin{aligned} \frac{\partial Q}{\partial s} + q_{c,O} - q_{c,I} &= 0 \\ \frac{\partial (Qc)}{\partial s} + c q_{c,O} - c_I q_{c,I} &= 2\pi r R \end{aligned} \tag{13}$$

where Q is conduit volumetric flux rate [$L^3\ T^{-1}$], c the calcium concentration [$M\ L^{-3}$], s the spatial coordinate in the direction parallel to the conduit [L], and $q_{c,O}$ and $q_{c,I}$ are the conduit sink and source terms [$L^2\ T^{-1}$], respectively. In these equations, calcite is only transported by advection.

Assuming laminar flow, the conduit volumetric flux rate is given by the Poisseuille equation:

$$Q = -\frac{g\pi r^4}{8\upsilon}\frac{\partial h}{\partial s} \tag{14}$$

where h is the hydraulic head [L] and g is the gravitational acceleration constant [$L^2\ T^{-1}$]. In this study, we use $g = 9.8$ m^2 s^{-1}. Turbulent flow in the conduits is often described by the Darcy-Weisbach equation. Using the friction factor from the Colebrook-White equation, the conduit volumetric flux rate can be expressed as

$$Q = -3.86 r^2 \sqrt{\alpha} \ln\left(\frac{\varepsilon}{7.4r} + \frac{0.89\upsilon}{2r\sqrt{\alpha}}\right)\frac{\partial h/\partial s}{|\partial h/\partial s|} \tag{15}$$

where ε is the rugosity [L] and v is the kinematic viscosity [$L\ T$]. To avoid switching between laminar and turbulent conduit equations using the Reynolds number, we use the full-range pipe-flow equation as proposed by *Swamee and Swamee* [2007]. This equation allows a smooth transition between laminar and turbulent conduit flow using a single equation (see Figure 3):

$$Q = -4r^2\sqrt{\alpha}\left\{\left(\frac{128\upsilon}{2\pi r\sqrt{\alpha}}\right)^4 + 1.153\left[\left(\frac{415\upsilon}{2r\sqrt{\alpha}}\right)^8 - \ln\left(\frac{\varepsilon}{7.4r} + \frac{1.775\upsilon}{2r\sqrt{\alpha}}\right)\right]^{-4}\right\}^{-1/4}\frac{\partial h/\partial s}{|\partial h/\partial s|} \tag{16}$$

The reaction surface per unit volume of porous limestone is typically very large and water entering the porous matrix quickly becomes saturated with respect to calcite. Therefore, in the model presented here it is assumed that the dissolution rate in the porous matrix is zero and thus that the calcium concentration in the water within the porous matrix equals the saturation equilibrium concentration for calcium c_{eq}. Following the quasi-stationary state approximation flow and solute transport in the matrix is given by

$$\begin{aligned} \nabla \cdot \mathbf{q} + q_{m,O} - q_{m,I} &= 0 \\ c &= c_{eq} \end{aligned} \tag{17}$$

where $\mathbf{q}$ the darcy flux vector [$L\ T^{-1}$] and $q_{m,O}$ and $q_{m,I}$ are matrix sink and source terms, respectively [T^{-1}]. Assuming variably saturated conditions and an isotropic hydraulic conductivity field, the darcy flux vector is given by

$$\mathbf{q} = -k_r K \nabla h \tag{18}$$

where k_r represents the relative permeability that depends on the saturation S by means of a retention curve and K the hydraulic conductivity [$L\ T^{-1}$].

Table 1. Parameters for Computing Calcite Dissolution Following *Kaufmann* [2009]

Parameter	Value
ω (mol kg^{-1})	10
ρ (kg m^{-3})	2700
k_s (mol m^{-2} s^{-1})	4E-7
c_{eq} (mol m^{-3})	2.0
n	4
υ (m^2 s^{-1})	1E-6
D_m (m s^{-1})	1E-9

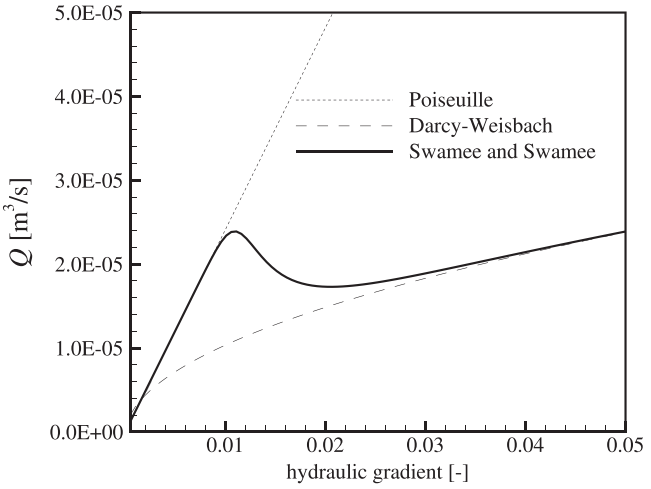

Figure 3. Volumetric flow rate in a straight conduit with $r = 0.005$ m and $\varepsilon = 0.001$ m according to equation (16) showing the smooth transition between laminar and turbulent flow as hydraulic gradient in pipe increases (solid line). Poisseuille equation for laminar flow (dotted line) and Darcy-Weisbach equation for turbulent flow (dashed line) are also shown for comparison.

2.5. Hydraulic Versus Catchment Control

As mentioned in section 1, a karst aquifer typically switches from hydraulic to catchment control as the drainage capacity of the conduit network increases. We thus need an approach to define proper flow boundaries along the land surface. We base this approach on the observation that in the absence of local depressions overland flow is typically characterized by relatively shallow depths. Because surface and subsurface hydraulic heads must be equal along the land surface, it follows that in the absence of local depressions, the maximum hydraulic heads along the land surface must roughly equal the land surface elevation. This estimation is also used by *Rehrl et al*. [2008] to simulate discharge from a karst aquifer under hydraulic control. However, inside local depressions, the surface water depth can be substantial and consequently the maximum hydraulic heads along the surface inside these depressions exceed the land surface elevation. Nonetheless, these hydraulic heads are ultimately limited to a value at which surface water will spill from the depression. Therefore, we propose to simulate the switch between hydraulic and catchment control using the concept of a spill elevation. The spill elevation is defined here as the surface water elevation at which surface water is routed toward the lateral model boundaries as illustrated in Figure 4. The spill elevation provides a reasonable approximation of the maximum subsurface hydraulic heads along the land surface that could occur. Thus, the spill elevation provides the hydraulic heads along the surface to specify hydraulic control. Catchment control occurs when the water table along the land surface is below the spill elevation. Values for the spill elevation are derived from a digital elevation model by a procedure proposed by *Wang and Liu* [2006]. It is noted that the switch between hydraulic and catchment control is a function of the topography and that in this study we assume that this topography is constant. Nonetheless, the underlying basics will not change if the topography changes with time and a change topography would simply require a new computation of the spill heights.

2.6. Numerical Implementation

By denoting the set of conduit and matrix cells connected to a conduit or matrix cell i with η_i, the discretized equations for steady state flow can be written in the following general form:

$$g_i = \sum_{j \in \eta_i} T_{ij}\left(h_i - h_j\right) + Q_i = 0 \tag{19}$$

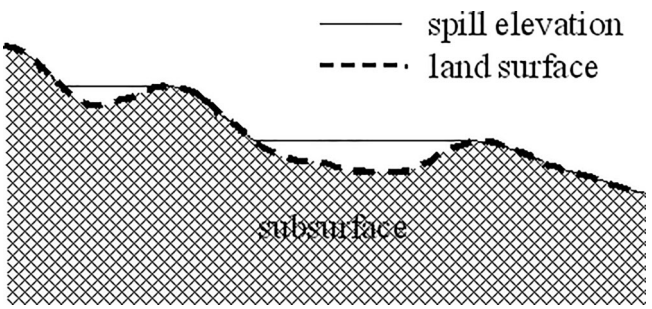

Figure 4. Spill elevation representing the elevation at which surface water flow is initiated toward lateral model boundaries.

where T_{ij} is a conductance term associated with the connection between cell i and cell j Q_i is a term to collect sink and source terms for a conduit or matrix cell i. For connections between matrix cells, harmonic weighting of hydraulic conductivities is used to obtain the conductance term. Between conduit cells, the conductance term is obtained by a harmonic weighting of conduit diameters. The exchange flux between a conduit cell and a matrix

cell is computed with the Peaceman well-index [*Peaceman*, 1983] which depends on the conduit radius, the hydraulic conductivity of the matrix cell as well as on the size of the matrix cell. This is different from most existing discrete-continuum models in which the coupling of conduit-matrix flow is governed by a constant lumped exchange parameter [*Liedl et al*., 2003; *Shoemaker et al*., 2008]. As discussed by *de Rooij et al*. [2013], the Peaceman well-index decreases the dependency of the computed exchange fluxes on the sizes of the matrix blocks surrounding the conduits.

Unconfined flow conditions in the porous medium model may be computed using Richards' equation in combination with for example the Van Genuchten-Mualem model [*Van Genuchten*, 1980]. However, this would yield a highly nonlinear scheme. Therefore, we adopt a common pseudo-constitutive relationship for the saturation S such that the saturation varies linearly between zero when the hydraulic head is at or below the matrix cell bottom and one when the hydraulic head is at or above the top of the matrix cell [*Bedekar et al*., 2012; *Keating and Zyvoloski*, 2009; *Panday and Huyakorn*, 2008]. If we define $k_r = S$ and apply upstream weighting, it follows that the horizontal transmissibility term scales linearly with the wetted thickness of the upstream matrix cell. Linear variation of the wetted thickness fraction between zero and one is smoothed to avoid slope discontinuities at zero and unity. The smoothing function used in our model is similar to the one used in MODFLOW [*Panday et al*., 2013]. We follow the approach of *Panday and Huyakorn* [2008] and keep the relative permeability constant at unity when computing vertical conductance terms. Since we assume fully saturated conditions in the conduits, unconfined conditions are only permitted in layers that lie above the conduit network.

Limiting the subsurface hydraulic heads along the land surface to the spill elevation in the numerical model is accomplished by applying drains to the topmost subsurface cells. The flux rate [$L\ T^{-1}$] associated with these drains is

$$q=\begin{cases}\gamma(h_t-h_{se}) & \text{if } h_t > h_{se}\\ 0 & \text{if } h_t \le h_{se}\end{cases} \tag{20}$$

where h_t is the hydraulic head in a topmost cell, h_{se} the spill elevation associated with the drain, and γ is the drain conductance term [T^{-1}]. Using Darcy's Law, the drain conductance term is computed using $\gamma=2K/\Delta z$, where K and Δz are the hydraulic conductivity and the vertical cell size of a topmost matrix cell, respectively.

For the conduits, the set of discretized equations governing steady state reactive transport can be written as

$$g_i=\sum_{j\in\eta_i^*} G_{ij}\left(c_i-c_j\right)+\left(q_{c,I}c_I-q_{c,O}c_i\right)\Delta s_i-2\pi r_i R(c_i)\Delta s_i=0 \tag{21}$$

where η_i^* is the set of conduit cells adjacent to a conduit cell i and Δs_i is the length of conduit cell i. The term G_{ij} is an advection term. Using upwinding this term is given by

$$G_{ij}=\begin{cases}Q_{ij} & \text{if} \quad h_i < h_j\\ 0 & \text{if} \quad h_i \le h_j\end{cases} \tag{22}$$

where Q_{ij} is the computed steady state volumetric flux between cells i and j. For the matrix, the set of discretized equations is simply given by

$$g_i=c_i-c_{eq}=0 \tag{23}$$

The discretized flow and reactive-transport equations are solved using the Newton-Raphson procedure and a preconditioned biconjugate gradient stabilized method. After each iteration, flow as well as reactive-transport solutions are updated with the adaptive underrelaxation scheme of *Cooley* [1983].

Our reactive-transport scheme differs from the scheme in most existing speleogenesis models where the calcite concentrations are solved from upstream to downstream using [*Dreybrodt*, 1996]:

$$c_i=c_{in}+2\pi r_i R(c_{in})\Delta s_i/Q_{in} \tag{24}$$

where Q_{in} is the total volumetric flux entering cell i and c_{in} is the concentration of the inflowing water assuming complete mixing. Since the reaction rate is linearized by using the known concentration of the

water flowing into the cell, no iteration procedure is required for this method. However, the drawback of this explicit scheme is that if Δs_i is not sufficiently small, then a cell can become saturated with respect to calcite while the water flowing into the cell is not yet saturated. This effect is known as numerical saturation. To avoid numerical saturation with the scheme defined by equation (24), the solute transport problem is typically solved using a finer discretization with respect to the one being using to solve the flow problem.

In our implicit scheme, numerical saturation with respect to calcite cannot occur. As indicated in equation (21), the reaction rate R in a conduit cell i is a function of the calcite concentration within cell i. If a cell is saturated with respect to calcite, then the production rate of calcite due to dissolution is zero (i.e., $R(c_{eq})=0$). Hence, the water flowing into the cell must have been saturated otherwise it is not possible to reach saturation with respect to calcite. Since numerical saturation cannot occur, our model uses the same spatial discretization for solving reactive transport as the one used for solving flow.

After solving the solute transport problem, the reaction rates are known for all the conduit transport cells. The increase in conduit radius during a time step Δt can then be computed using:

$$\Delta r_i = R_i \Delta t / \rho \omega \tag{25}$$

3. Verification

In this section, we consider two idealized simulation scenarios to verify our model against previous simulations. Following a simulation example of *Dreybrodt* [1996], we specify a single horizontal conduit with a length of a 1000 m and a radius of 2E-4 m. The surrounding matrix is not accounted for and we use $c^* = 1.6$ mol/m^3. Fixed hydraulic heads are specified at both ends of the conduits defining an initial hydraulic gradient is 0.05. Water flowing into the conduit has a zero concentration with respect to calcite. In our model, we discretize the conduit uniformly into 1000 cells and the applied dissolution time step is 1 year. Other model parameters are given in Table 1. Figure 5 shows the flow rate at the outflow end of the conduit as a function of time. Similar to *Dreybrodt* [1996], our model predicts a breakthrough at around 17,000 years, where breakthrough is defined by the time that the flow rate at the outflow end of the conduit increases several orders of magnitude. Figure 5 also illustrates our model results for an example presented by *Kaufmann* [2009], which is very similar to the above example of Dreybrodt, but with an initial head gradient of 0.01, a radius of 5E-4 m and $c^* = 1.8$ mol/m^3. Similar to *Kaufmann* [2009], our model predicts a breakthrough time of about 19,000 years.

To illustrate the effect of flow exchange with a surrounding matrix on the breakthrough time, we consider a model domain similar to the one simulated by *Kaufmann* [2003]. The matrix dimensions are defined by a length of 742.4 m in the x direction, a width of 382.5 m in the y direction, and a height of 1 m in the z direction. A horizontal conduit is placed in the center along the length of the matrix domain. Contrary to *Kaufmann* [2003], we do not consider an additional network of finer conduits surrounding the main central conduit. The matrix is discretized into a single layer of cells with a length and a width of 7.5 m. The conduit is discretized into cells with a length of 7.5 m. An initial head difference of 100 m along the length of the domain is specified by means of fixed heads at both ends of the model. Water flowing into the conduit has a zero concentration with respect to calcite. The initial radius of the conduit is 2E-4 m and the hydraulic conductivity of the matrix is varied over a similar range as *Kaufmann* [2003]. The applied dissolution time step is 1 year.

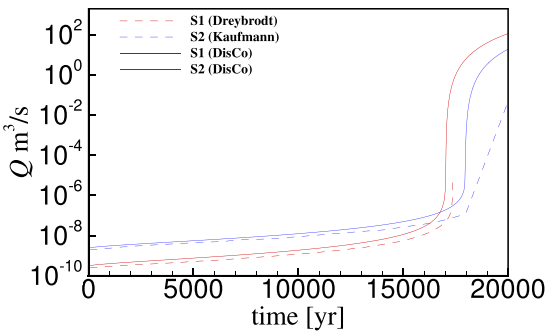

Figure 5. Simulated flow rates at the outflow boundary of a single conduit. S1: example of *Dreybrodt* [1996]. S2: example of *Kaufmann* [2009].

Figure 6 illustrates the breakthrough times predicted by our model. These results reproduce the findings of *Kaufmann* [2003] and *Bauer et al.* [2003] that breakthrough times are faster when the matrix is accounted for. In essence, if a surrounding matrix is accounted for, then the flow rate through the upstream parts of the conduit is no longer limited by the smaller conduit diameters downstream as water can flow from the

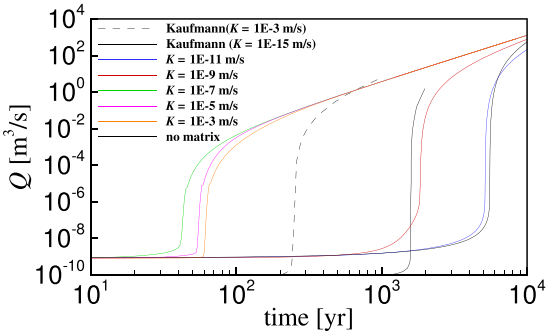

Figure 6. Simulated flow rates at the outflow boundary of a single conduit for different hydraulic conductivities of the surrounding matrix. Minimum and maximum breakthrough times as simulated by *Kaufmann* [2003] are also illustrated.

conduit into the matrix. Consequently, more water with a zero concentration of calcite can enter the conduit and this increases the dissolution rates. The equipotential lines at 50 years for a matrix hydraulic conductivity of 1E-7 m/s, as illustrated in Figure 7b, clearly indicate that there is flow from the conduit into the matrix.

Kaufmann [2003] and *Bauer et al*. [2003] found that increasing the matrix hydraulic conductivity results in faster breakthrough as more water flows from the conduit to the matrix. Our results, confirm these finding but only up to a matrix hydraulic conductivity of 1E-7 m/s. As illustrated in Figure 6, a further increase in the matrix hydraulic conductivity results in a modest increase in breakthrough times compared to the minimum breakthrough time obtained with a matrix hydraulic conductivity of 1E-7 m/s. To explain this behavior it is observed that if the matrix hydraulic conductivity is sufficiently small, then enlarged conduits will have a strong effect on the equivalent porous medium hydraulic conductivity of the combined conduit-matrix system. Consequently, when the upstream conduit cells are being widened, the contrast in this equivalent hydraulic conductivity between the upstream and downstream part of the flow domain is increased. Therefore, the hydraulic gradient across the downstream conduit segment is increased and this increases the amount of water flowing through this segment. As illustrated in Figure 7b a matrix hydraulic conductivity of 1E-7 m/s yields a relatively steep hydraulic gradient across the downstream part of the conduit after 50 years of dissolution. Figure 7b also shows that for increased matrix hydraulic conductivities, the hydraulic gradient across the downstream conduit segments remains closer to the initial gradient. This is because enlarged conduits have a smaller effect on the equivalent hydraulic conductivity if the matrix hydraulic conductivity is sufficiently large. A smaller gradient implies less water flowing through the downstream conduit segments and thus breakthrough times increase. Compared to *Kaufmann* [2003], we find that the maximum breakthrough times obtained when the matrix is not accounted for or when the matrix has a negligible effect are larger, while the minimum breakthrough times are smaller. The reasons for these differences are not clear. Since, we can reproduce the model results of *Dreybrodt* [1996] and *Kaufmann* [2009] for a single conduit without a matrix, we are confident that the maximum breakthrough time simulated in our second example is accurate.

4. Application

To illustrate that our hydrochemical model can generate a realistic conduit network, we apply our model to a karst region in Florida, USA, along the Suwannee River. The extent of our model domain is defined by the adjacent springsheds of Fanning Springs and Manatee Springs. The combined extent of these two springsheds is taken from *Farrell et al*. [2005] and is depicted in Figure 8. In the model region, the Upper Floridan

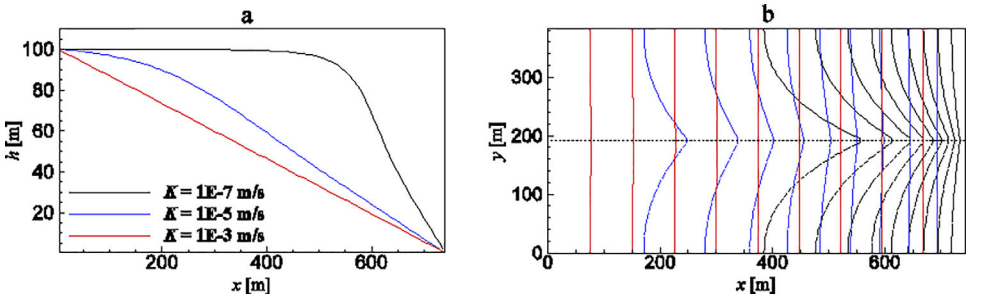

Figure 7. (a) Hydraulic heads in the conduit and (b) corresponding equipotential lines of hydraulic heads in the matrix after 50 years for selected values of the matrix hydraulic conductivity. The equipotential lines are plotted with an interval of 10 m with $h = 100$ m at $x = 0$ m and $h = 0$ m at $x = 742.5$ m.

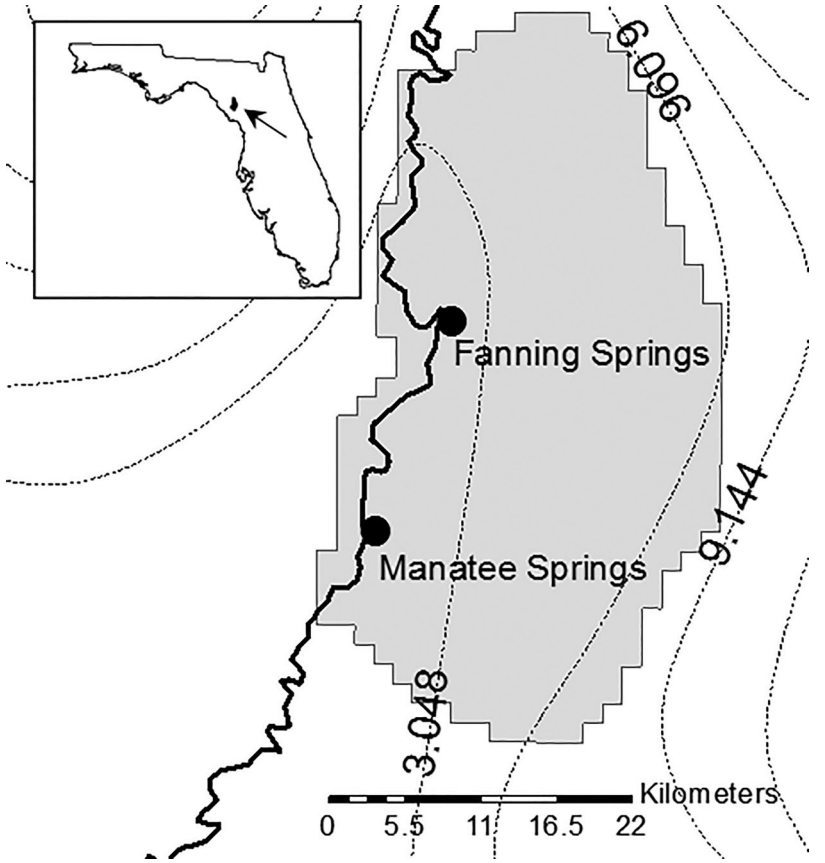

Figure 8. Model region (grey) along Suwanee River (thick black line) with the two springs (black dots). Potentiometric map (m) from predevelopment period (www.dep.state.fl.us) is provided by dashed black lines. In the top left corner, the location of the model region within the state of Florida is provided.

Aquifer consists of unconfined karstified limestones overlain by the sandy Surficial Aquifer. The Upper Floridan Aquifer is an eogenetic karst aquifer characterized by a relatively high porosity and a relatively high hydraulic conductivity in the porous matrix [*Langston et al*., 2012]. The average discharge of Fanning Springs and Manatee Springs during the last few decades has been about 2.5 m^3/s and 5 m^3/s, respectively [*Farrell et al*., 2005].

Subsequent lowering of the sea level during the Quaternary played an important role in the karst evolution in this region as it involved the gradual exposure of the land surface exposure of the carbonate rocks that make up the Upper Floridan [*Denizman and Randazzo*, 2000]. Initial voids in the rocks may have originated from previous episodes of land surface exposure during the Oligocene as well as from fracturing during the early Miocene [*Denizman and Randazzo*, 2000].

Our example model contains four layers. The first layer is the Surficial Aquifer and the underlying three layers represent the Upper Floridian Aquifer, obtained by dividing the Upper Floridan Aquifer into three layers with equal thicknesses. The Surficial Aquifer consists of siliciclastic sediments of Miocene age. The thicknesses of the Surficial Aquifer and the Upper Floridian Aquifer were taken from USGS data [*Williams and Dixon*, 2015]. Each layer is discretized into cells with lateral dimensions equal to 200 m. The land surface elevation was derived from a digital elevation models with a spatial resolution of 30 m (ned.usgs.gov). For this example, it is assumed that this elevation remains constant during the simulation of conduit dissolution.

A hydraulic conductivity of 1E-4 m/s is specified for the Upper Floridan Aquifer, which in our model results in an average transmissivity of about 210 m^2/d. This is relatively very small compared to the range from 150 to 100,000 m^2/d based on aquifer tests in the region [*Grubbs and Crandall*, 2007]. However, those measured values reflect the bulk transmissivities of the aquifer, whereas we distinguish between the matrix and the

conduits within this aquifer. For the Surficial Aquifer, we assume a hydraulic conductivity of 1E-2 m/s, a typical value for sandy aquifers. The top of the model is recharged with a rate of 2E-8 m/s. Assuming that most of the applied recharge will eventually percolate into the Upper Floridan Aquifer, this would yield a recharge of the Floridan Aquifer of about 0.63 m/yr. This is a reasonable value with respect to current conditions. Namely, in areas where the Upper Floridan Aquifer is unconfined, such as our model region, the recharge into the Upper Floridan Aquifer is relatively high and varies between 0.4 and 0.8 m/yr [*Grubbs*, 1998]. In this example, it is assumed that the recharge remains constant during the dissolution process and does not differ from its current value.

To enable karstification within the Upper Floridan Aquifer, we arbitrarily define a random initial proto-conduit network within the third model layer such that it is located in the middle of the Upper Floridian Aquifer. This network is based on two sets of proto-conduits each consisting of 3000 line segments. The orientation is defined by a uniform probability distribution function where the orientation varies between 43° and 47° for the first set of segments and between −43° and −47° for the second set. The lengths of the proto-conduits follow a gamma distribution function with shape parameter $k = 1.2$ and a scale parameter $\theta = 1000$. Conceptually, the initial conduit network accounts for the voids originating from previous episodes of karstification during subaerial exposure in the Oligocene as well as from fracturing during the early Miocene.

To condition our model to the known spring locations, we define fixed hydraulic heads at those locations within the network that correspond most closely to the spring locations. These Dirichlet flow boundary conditions are set to 1.5 and 2.5 m for the Fanning Springs and Manatee Springs, respectively. These values are close to the average stages in modern times as measured at the springs [*Farrell et al*., 2005]. Three hundred vertical preferential flow paths are defined by generating *x* and *y* values for 300 points within the rectangle enclosing the model region using uniform probability distribution functions. We only place these flow paths at locations where the spill height elevation exceeds the maximum hydraulic head at the springs. Otherwise, certain vertical flow paths with a low spill height may outcompete the springs during the evolution of the conduit network in terms of discharge. The initial conduit diameters were set to 1E-3 m. Figure 9 illustrates the overall model geometry. Figure 10 illustrates the initial proto-conduit network and the random locations of the vertical preferential flow paths. For this example, we assume that the concentration of calcite of water entering the conduits via the vertical preferential pathways equals 1.5 mol/m^3. The applied dissolution time step is a hundred years and $c^* = 1.8$ mol/m^3. Other parameters are specified in Table 1.

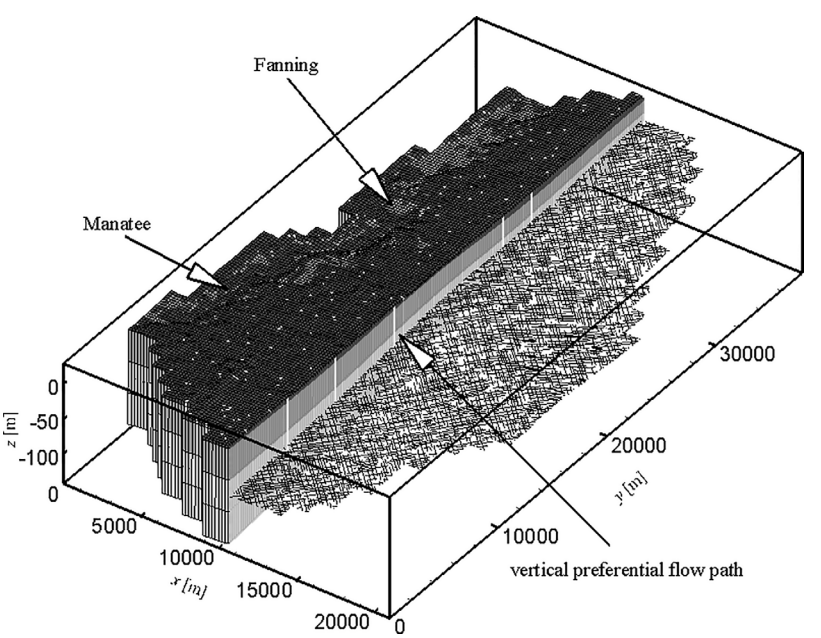

Figure 9. Model geometry.

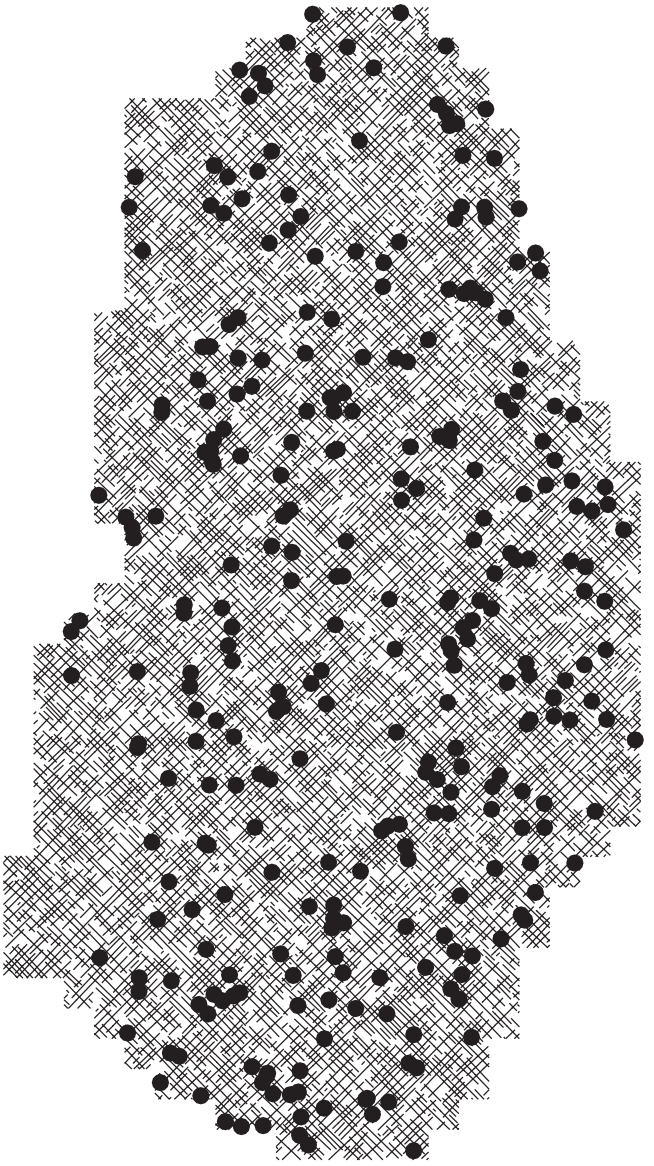

Figure 10. Initial network and placement of vertical preferential flow paths (black dots).

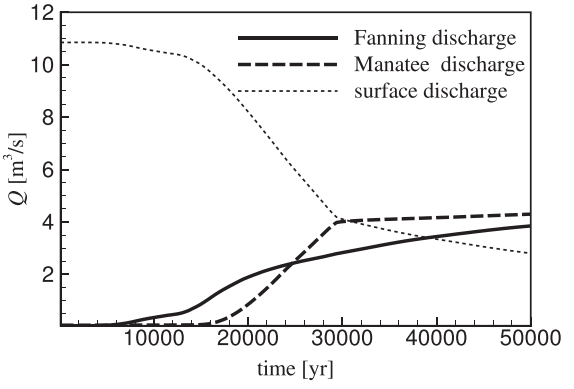

Figure 11. Evolution of spring and surface discharge during conduit evolution.

Figure 11 shows the simulated discharges over the simulation period at the springs as well as the aggregated discharge at the land surface depending on the spill elevation. The simulated discharge at Manatee Springs and Fanning Springs are slightly below and above reported values of 5 and 2.5 m^3/s, respectively. Figure 12 illustrates the evolution of the conduit network at several stages during a 50,000 year simulation period as well as the evolution of hydraulic head field in the matrix. The simulated hydraulic head field is relatively close to the potentiometric map for the predevelopment period as depicted in Figure 8. The simulation ran in 25 min on a standard laptop (Intel i7-6820HQ 2.7 GHz).

In this simulation, it takes about 20,000 years to develop a well-connected conduit network, a value that is comparable with the time to create regional networks as reported by *Kaufmann* [2009]. The global topology of the final network is a typical branchwork, but around the main branches local maze type networks are present. From Figure 11, it can be observed that around 30,000 years, there is a sudden change in the slope of the discharge versus time plot for the Manatee Spring. This change happens because at this time the Manatee Spring has outcompeted the drains associated with the spill elevation in its surroundings. Further but slower increase in discharge is thereafter accomplished by competition with Fanning Springs. Nonetheless, the discharge at Fanning Springs still increases over time by competing with remaining surface drains in its surroundings.

The last simulated steady state flow field and the last computed conduit diameters may be used to simulate transient backward solute transport (in both the conduits and the matrix) using a reversed velocity field and a unit pulse at the springs. For the transient transport simulation, we must add a storage term to the advection

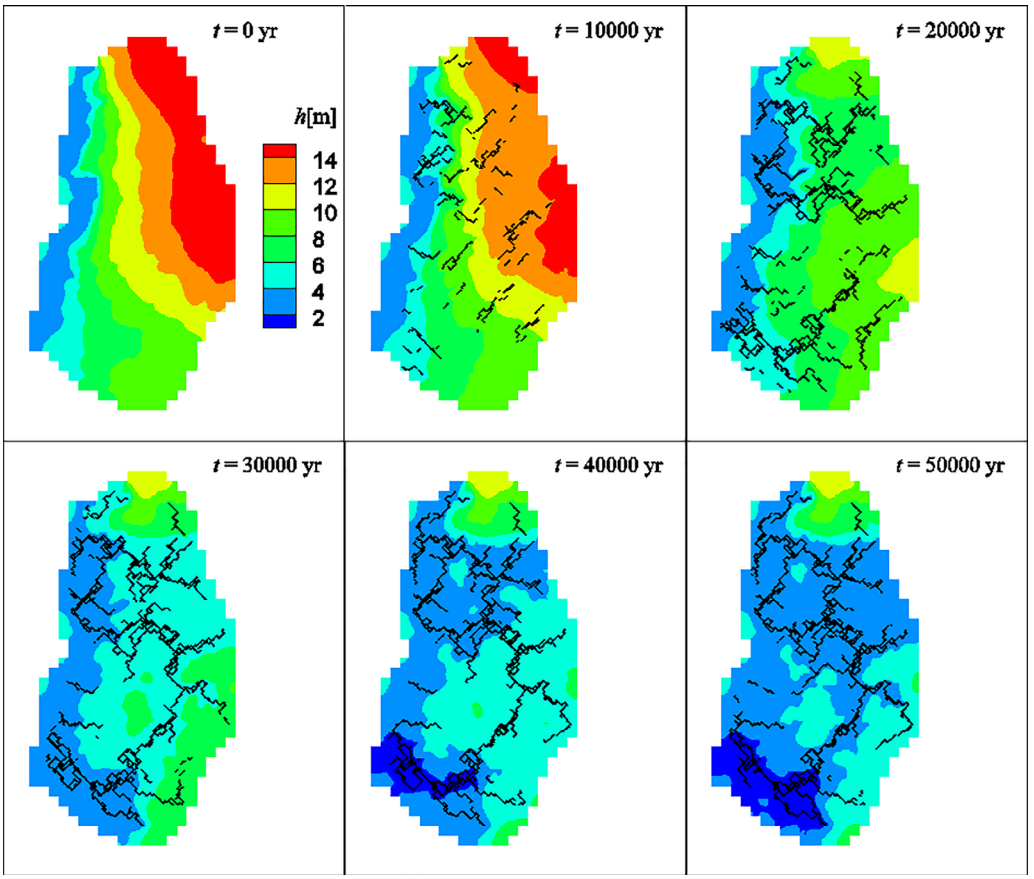

Figure 12. Evolution of the conduit network and the hydraulic head field in model layer containing the network (third model layer). Only conduits with $Q > 0.1$ m^3/s are shown.

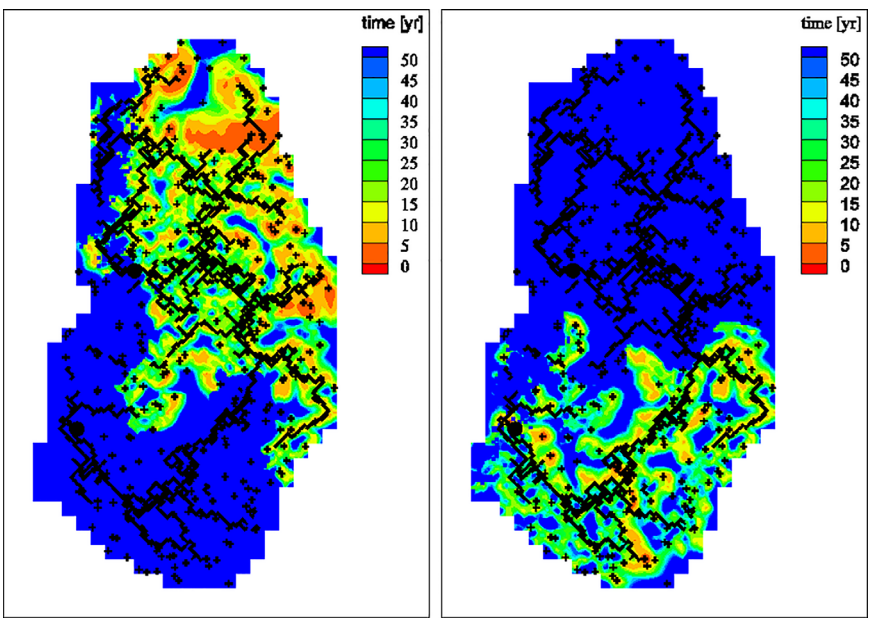

Figure 13. Mean travel time to reach (left) Fanning Springs and (right) Manatee Springs based on evolved conduit network. Only conduits with $Q > 0.1$ m^3/s are shown. Vertical preferential flow paths are shown with plus symbols. The two springs are shown as black dots.

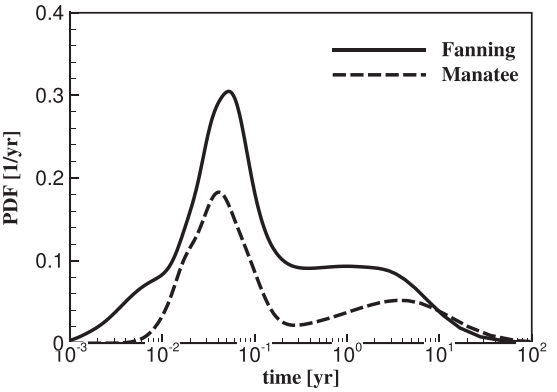

Figure 14. Residence time distribution of water discharging at the springs.

scheme which depends on the water content requiring the matrix porosity as an additional parameter. For our simulation, we assume a porosity of 0.1 in the matrix. To allow relatively high velocities along the vertical preferential flow paths, the matrix cells representing these paths are assigned a porosity of 0.001. Backward transport simulations provides useful information about the vulnerability of groundwater systems [*Cornaton and Perrochet*, 2006; *Molson and Frind*, 2012]. Here we use the backward transport simulations to obtain the mean travel times to reach the spring along the recharge boundary as depicted in Figure 13. The mean travel times are highly variable and are relatively small near the conduit network and near the locations of the preferential vertical flow paths, indicating that these are vulnerable areas with respect to contaminant transport toward the springs. From the same simulations, we also obtain the probability distribution function of the groundwater residence time of the water discharging at the springs as shown in Figure 14. The groundwater residence time pdf is bimodal. This bimodality is associated with concentrated versus diffuse recharge into the conduit system. Namely, the focused recharge component arrives earlier than the diffuse recharge component. The obtained average groundwater residence time is 20 years for Fanning Springs and 30 years for Manatee Springs. These simulated values fall within the range of measured values which lie between 15 and 30 years [*Happell et al*., 2006; *Katz*, 2004].

5. Discussion

Because a speleogenesis model accounts for the positive feedback mechanism responsible for the hierarchical conduit structure, it has potential to be used as a tool to generate conduit networks with realistic connectivity patterns. We introduce two significant improvements that facilitate this type of application of a speleogenesis model.

First, we propose an innovative physically based algorithm based on the concept of a spill elevation that permits an automatic and fully implicit switch between hydraulic and catchment control. The algorithm is physics based in so far as the spill elevation is a reasonable approximation for the maximum subsurface hydraulic heads along the land surface. In the model, the switch is simulated using a head-dependent drain acting on the topmost matrix cells. This nonlinear drain permits the model to compute fully implicitly the smooth transition from hydraulic to catchment control for each cell separately. The switch is fully controlled by the spill elevation and the drain conductance term and does not require additional switch parameters as used in previous models [*Bauer et al*., 2005]. Thus, if the topography is known our switch algorithm is fully defined and therefore its implementation is relatively simple. Moreover, since the algorithm is physically based, it enforces physically realistic flow boundaries. Even if the actual flow boundaries during conduit evolution cannot be reconstructed accurately, it can be argued that it is important that the applied flow boundaries are at least reasonable in a physical sense.

Second, our spelogenesis model avoids numerical saturation by applying an implicit reactive-transport scheme in which the reaction rate is evaluated at the conduit cell centers. This is advantageous as it permits larger conduit cells and which yields improved computational efficiency. In fact, for flow and reactive-transport, we apply the same spatial discretization. This simplifies the modeling to a significant extent, albeit at the expense of introducing nonlinear reactive-transport equations, as the reaction rate in our model depends on the calcite concentrations in the conduit cells.

Numerically, the accuracy of the model depends on the applied spatial discretization, the size of the dissolution time step and is affected by the numerical dispersion introduced by an upwind scheme. Although the issue of numerical accuracy deserves further study, it is noted that the effects of numerical inaccuracies of the model are likely to be small compared to uncertainty about the model input parameters as well as the

fact that our model does not account for a series of processes that may play a significant role in speleogenesis. Examples of such processes are mechanical erosion and sediment deposition within the conduits, the possible collapse of conduits, geomorphological processes that change the topography, and changes in climate conditions. Moreover, our model only accounts for dissolution processes in phreatic conduits and does not consider the effects of calcite dissolution in the vadose zone. As such it is clear that there remain many unresolved challenges in speleogenesis modeling.

Our case study illustrates that our model can generate a possible conduit network that yields reasonable result in terms of spring discharges, regional variation in hydraulic heads, and estimated groundwater residence times. The underestimated discharge at Manatee Springs may indicate that its actual springshed extends beyond the model region. Likewise, a decrease in the springshed of Fanning Springs may improve upon the overestimated discharge at Fanning Springs. However, the main objective of our application is to provide a proof of concept in the sense that our model can be used as a tool to generate conduit networks. Further tuning of the model to match field observations is beyond the scope of this paper.

The conduit network as simulated in our case study depends on a series of assumptions regarding for example the initial conduit network, the density of vertical preferential flow paths, the hydraulic conductivity values for the matrix, the applied flow boundary conditions, and the topography. We used a random initial network as well as random preferential vertical flow paths. However, if our model is applied to a region where actual observations are available, then it would be straightforward to condition the proto-conduit network or the preferential vertical flow paths to these observations. As shown in our case study, the model can be conditioned to known spring locations by defining Dirichlet flow conditions at corresponding locations within the network. Whereas we based the hydraulic conductivities in the matrix layers on reasonable estimates, these values could also be varied based on field evidence or geostatistical approaches. The recharge conditions can also be based on data from the paleoclimatic record if such data are available. As shown by the work of *Kaufmann* [2009], the model may be developed further to account for a change in topography during the simulation period. Such changes may affect the dissolution process as the flow boundaries in our model depend on the topography. Moreover, if topography changes due to erosion or deposition significant changes in the subsurface geometry may also occur.

Since our model depends on the input parameters regarding the initial conduit network, the density of vertical preferential flow paths, the hydraulic conductivity values for the matrix, the applied flow boundary conditions, and the topography which are often highly uncertain, it would be reasonable to randomly vary the model input parameters based on appropriate probability functions using a stochastic approach. Such an approach would serve two purposes. First, such a variation would permit a sensitivity analysis of the model to identify which model parameters or combination thereof most significantly influence the evolution of a conduit network. Second, by varying the model input parameters an ensemble of conduit networks is obtained and uncertainty in flow and transport predictions over the ensemble of networks can be examined.

It can be expected that if focused recharge occurs as in our case study, then a smaller matrix hydraulic conductivity may restrict diffusive infiltration into the matrix and may thus enhance the amount of water that infiltrates as focused recharge which would lead to more conduit development. It can be hypothesized that the initial connectivity and density of the initial network, the initial conduit diameters as well the number and parametrization of the vertical preferential flow paths will have a profound influence on conduit development. For example, more vertical preferential flow paths may result in more branches as there will be more locations where dissolution can start. Moreover, the density and connectivity of an evolved network is likely limited by the density and connectivity of the initial network. These effects will be analyzed using formal global sensitivity analysis in forthcoming studies.

Although our case study illustrates that we can generate a visually realistic conduit connectivity pattern, it would also be interesting in future studies, to analyze the topology of the networks as generated by our model in terms of appropriate statistical metrics. Several methods exist that would enable such an analysis [*Collon et al*., 2017; *Hendrick and Renard*, 2016]. Such an analysis could provide a more rigorous proof that our tool is able to generate realistic conduit patterns. Moreover, in combination with a sensitivity analysis, it could also provide insights into factors that determine the topology of conduit networks.

Although a common argument for using a heuristic erosion potential in process-based approaches is based on limiting the computational efforts, the reactive-solute transport step in the presented model is not particularly computationally demanding. This step is simulated assuming steady state conditions and is

typically less demanding than the computation of a steady state flow field. Compared to the model approach of *Lafare* [2012], we believe that our model requires similar computational effort since in that model the reactive-solute transport step is replaced with a groundwater age computation step. The approach of *Borghi et al*. [2012] is likely to be significantly more computationally efficient. Namely, that approach avoids flow simulations and instead relies on generating preferential flow paths using a fast-marching algorithm. As discussed by *Borghi et al*. [2012], simulating the flow field increases the computational effort of their approach. Moreover, the number of iterations between updating and the eroding the preferential flow paths is typically low, particular with respect to the number of dissolution time steps in our model. In their approach, the first iteration already defines a complete conduit connection between an inlet and an outlet. Subsequently, a next iteration will add additional conduits that typical connect to the resulting network from a previous iteration. Although their approach results in realistic and hierarchical networks, the positive feedback between flow and conduit widening is simulated in a very discrete fashion in which conduits form one after the other. In reality, this positive feedback is a continuous mechanism. As such it may be argued that a model like the one presented here which makes many more iterations between flow and dissolution could result in more realistic networks albeit at the expense of increased computational efforts.

A significant strength of our model is that it generates a conduit network that can be readily applied in a flow or solute transport model. This is evident since flow and solute transport are being computed during the speleogenesis simulation. Moreover, directly after the simulation, the model provides spring discharges as well as the hydraulic head field. Therefore, the model directly provides criteria to select conduit networks that reproduce observed hydrologic behaviors of interest. Additional criteria could be obtained by subsequent flow and transport simulations. For example, solute transport simulations could be compared to tracer test data. As illustrated in our application, water age computations may be used to further investigate if the karst aquifer model is reasonable or not.

The main technical limitations of our model approach stem from the underlying model assumptions of phreatic conduits, a single inception horizon and a constant topography. Resolving these issues would require a more complex model than the model presented in this study. Other assumptions as used in our case study regarding recharge conditions, the geometry of the initial network and hydraulic parameters for the matrix may be relaxed if more data are available to quantify the model parameters.

6. Conclusion and Outlook

In this study, we presented a hydrochemical model with potential to generate realistic conduit networks that honor what is known about the geology, hydrogeology, and topography of a particular karst system. Compared to existing speleogenesis models, our model contains two significant improvements. First, our model accounts for the switch between hydraulic and catchment control during conduit evolution using a physics-based and implicit switching algorithm based on the concept of a spill elevation. Second, in our model, numerical saturation cannot occur such that reactive-solute transport can be solved using a coarser spatial discretization. As such, contrary to existing speleogenesis models, we can solve flow and reactive-solute transport on the same grid. Due to these improvements, we can apply the model on a regional scale.

Our model provides information such as the discharge at springs and the hydraulic head field to decide if a conduit network is reproducing adequately observed behaviors. Moreover, there is potential to obtain additional criteria such as groundwater residence times to select behavioral conduit networks. Ultimately, we seek to use our model to construct ensembles of possible conduit realizations within a stochastic framework. Use of such ensembles to simulate flow and transport through uncertain conduit networks will enhance the applicability of discrete-continuum models. In particular, quantification of model prediction uncertainty should enhance the applicability of such models as management tools.

Acknowledgment
The model codes or parts thereof can be obtained from the corresponding author.

References

Bauer, S., R. Liedl, and M. Sauter (2003), Modeling of karst aquifer genesis: Influence of exchange flow, *Water Resour. Res.*, *39*(10), 1285, doi: 10.1029/2003WR002218.

Bauer, S., R. Liedl, and M. Sauter (2005), Modeling the influence of epikarst evolution on karst aquifer genesis: A time-variant recharge boundary condition for joint karst-epikarst development, *Water Resour. Res.*, *41*, W09416, doi:10.1029/2004WR003321.

Bedekar, V., R. Niswonger, K. Kipp, S. Panday, and M. Tonkin (2012), Approaches to the simulation of unconfined flow and perched groundwater flow in MODFLOW, *Ground Water*, *50*(2), 187–198.

Beek, W., and K. Muttzall (1975), *Transport Phenomena*, John Wiley, New York.
Birk, S., R. Liedl, and M. Sauter (2006), Karst spring responses examined by process-based modeling, *Ground Water*, *44*(6), 832–836.
Borghi, A., P. Renard, and S. Jenni (2012), A pseudo-genetic stochastic model to generate karstic networks, *J. Hydrol.*, *414*, 516–529.
Borghi, A., P. Renard, and F. Cornaton (2016), Can one identify karst conduit networks geometry and properties from hydraulic and tracer test data?, *Adv. Water Resour.*, *90*, 99–115.
Collon, P., D. Bernasconi, C. Vuilleumier, and P. Renard (2017), Statistical metrics for the characterization of karst network geometry and topology, *Geomorphology*, *283*, 122–142.
Cooley, R. L. (1983), Some new procedure for numerical solution of variably saturated flow problems, *Water Resour. Res.*, *19*(5), 1271–1285.
Cornaton, F., and P. Perrochet (2006), Groundwater age, life expectancy and transit time distributions in advective-dispersive systems: 1. Generalized reservoir theory, *Adv. Water Resour.*, *29*(9), 1267–1291.
de Rooij, R., P. Perrochet, and W. Graham (2013), From rainfall to spring discharge: Coupling conduit flow, subsurface matrix flow and surface flow in karst systems using a discrete-continuum model, *Adv. Water Resour.*, *61*, 29–41.
Denizman, C., and A. F. Randazzo (2000), Post-Miocene subtropical karst evolution, lower Suwannee River basin, Florida, *Geol. Soc. Am. Bull.*, *112*(12), 1804–1813.
Dreybrodt, W. (1988), *Processes in Karst Systems, Physics, Chemistry and Geology*, Springer, New York.
Dreybrodt, W. (1996), Principles of early development of karst conduits under natural and man-made conditions revealed by mathematical analysis of numerical models, *Water Resour. Res.*, *32*(9), 2923–2935.
Dreybrodt, W., D. Romanov, and G. Kaufmann (2010), Evolution of caves in porous limestone by mixing corrosion: A model approach, *Geol. Croatica*, *63*(2), 129–135.
Eisenlohr, L., M. Bouzelboudjen, L. Kiraly, and Y. Rossier (1997a), Numerical versus statistical modelling of natural response of a karst hydrogeological system, *J. Hydrol.*, *202*(1–4), 244–262.
Eisenlohr, L., L. Kiraly, M. Bouzelboudjen, and Y. Rossier (1997b), Numerical simulation as a tool for checking the interpretation of karst spring hydrographs, *J. Hydrol.*, *193*(1–4), 306–315.
Farrell, M. D., J. Good, D. Hornsy, A. Janicki, R. Mattson, and S. Upchurch (2005), *MFL Establishment for the Lower Suwannee River and Estuary, Little Fanning, Fanning, and Manatee Springs*, Water Resource Associates Inc., Tampa.
Filipponi, M., P. Y. Jeannin, and L. Tacher (2010), Understanding cave genesis along favourable bedding planes. The role of the primary rock permeability, *Z. Geomorphol.*, *54*, 91–114.
Gabrovsek, F., and W. Dreybrodt (2001), A model of the early evolution of karst aquifers in limestone in the dimensions of length and depth, *J. Hydrol.*, *240*(3–4), 206–224.
Gabrovsek, F., and W. Dreybrodt (2010), Karstification in unconfined limestone aquifers by mixing of phreatic water with surface water from a local input: A model, *J. Hydrol.*, *386*(1–4), 130–141.
Gallegos, J. J., B. X. Hu, and H. Davis (2013), Simulating flow in karst aquifers at laboratory and sub-regional scales using MODFLOW-CFP, *Hydrogeol. J.*, *21*(8), 1749–1760.
Grubbs, J. W. (1998), *Recharge rates to the Upper Floridan Aquifer in the Suwannee River Water Management District, Florida*, U.S. Geol. Surv., Tallahassee, Fla.
Grubbs, J. W., and C. A. Crandall (2007), *Exchanges of Water Between the Upper Floridan Aquifer and the Lower Suwannee and Lower Santa Fe Rivers, Florida*, U.S. Geol. Surv., Reston, Va.
Hanna, R. B., and H. Rajaram (1998), Influence of aperture variability on dissolutional growth of fissures in karst formations, *Water Resour. Res.*, *34*(11), 2843–2853.
Happell, J. D., S. Opsahl, Z. Top, and J. P. Chanton (2006), Apparent CFC and H-3/He-3 age differences in water from Floridan Aquifer springs, *J. Hydrol.*, *319*(1–4), 410–426.
Hendrick, M., and P. Renard (2016), Fractal dimension, walk dimension and conductivity exponent of karst networks around Tulum, *Frontiers Phys.*, *4*, 27.
Hill, M. E., M. T. Stewart, and A. Martin (2010), Evaluation of the MODFLOW-2005 conduit flow process, *Ground Water*, *48*(4), 549–559.
Jaquet, O., P. Siegel, G. Klubertanz, and H. Benabderrhamane (2004), Stochastic discrete model of karstic networks, *Adv. Water Resour.*, *27*(7), 751–760.
Katz, B. G. (2004), Sources of nitrate contamination and age of water in large karstic springs of Florida, *Environ. Geol.*, *46*(6–7), 689–706.
Kaufmann, G. (2003), A model comparison of karst aquifer evolution for different matrix-flow formulations, *J. Hydrol.*, *283*(1–4), 281–289.
Kaufmann, G. (2009), Modelling karst geomorphology on different time scales, *Geomorphology*, *106*(1–2), 62–77.
Kaufmann, G., D. Romanov, and T. Hiller (2010), Modeling three-dimensional karst aquifer evolution using different matrix-flow contributions, *J. Hydrol.*, *388*(3–4), 241–250.
Keating, E., and G. Zyvoloski (2009), A stable and efficient numerical algorithm for unconfined aquifer analysis, *Ground Water*, *47*(4), 569–579.
Kiraly, L. (1985), FEM-301—A three dimensional model for groundwater flow simulation, in *NAGRA Tech. Rep. 84–49*, Nagra, Baden, Switzerland.
Kiraly, L. (1998), Modelling karst aquifers by the combined discrete channel and continuum approach, *Bull. Cent. d'Hydrogéol.*, *16*, 77–98.
Kiraly, L., P. Perrochet, and Y. Rossier (1995), Effect of epikarst on the hydrograph of karst springs: a numerical approach, *Bull. Cent. d'Hydrogéol.*, *14*, 199–220.
Kovacs, A., and P. Y. Jeannin (2003), Hydrogeological overview of the Bure plateau, Ajoie, Switzerland, *Eclogae Geol. Helv.*, *96*(3), 367–379.
Lafare, A. (2012), *Modélisation mathématique de la spéléogenèse: une approche hybride à partir de réseaux de fractures discrets et de simulations hydrogéologiques*, Sciences de la Terre. Université Montpellier II - Sciences et Techniques du Languedoc.
Langston, A. L., E. J. Screaton, J. B. Martin, and V. Bailly-Comte (2012), Interactions of diffuse and focused allogenic recharge in an eogenetic karst aquifer (Florida, USA), *Hydrogeol. J.*, *20*(4), 767–781.
Lichtner, P. C. (1988), The quasi-stationary state approximation to coupled mass-transport and fluid-rock interaction in a porous medium, *Geochim. Cosmochim. Acta*, *52*(1), 143–165.
Liedl, R., M. Sauter, D. Huckinghaus, T. Clemens, and G. Teutsch (2003), Simulation of the development of karst aquifers using a coupled continuum pipe flow model, *Water Resour. Res.*, *39*(3), 1057, doi:10.1029/2001WR001206.
Molson, J. W., and E. O. Frind (2012), On the use of mean groundwater age, life expectancy and capture probability for defining aquifer vulnerability and time-of-travel zones for source water protection, *J. Contam. Hydrol.*, *127*(1–4), 76–87.
Ortoleva, P., E. Merino, C. Moore, and J. Chadam (1987), Geochemical self-organization. 1. Reaction-transport feedbacks and modeling approach, *Am. J. Sci.*, *287*(10), 979–1007.
Palmer, A. N. (1991), Origin and morphology of limestone caves, *Geol. Soc. Am. Bull.*, *103*(1), 1–21.

Panday, S., and P. S. Huyakorn (2008), MODFLOW SURFACT: A state-of-the-art use of vadose zone flow and transport equations and numerical techniques for environmental evaluations, *Vadose Zone J.*, *7*(2), 610–631.
Panday, S., C. D. Langevin, R. G. Niswonger, M. Ibaraki, and J. D. Hughes (2013), MODFLOW-USG version 1: An unstructured grid version of MODFLOW for simulating groundwater flow and tightly coupled processes using a control volume finite-difference formulation, *U.S. Geol. Surv. Tech. Methods*, *Book 6, Chap. A45*, 66 pp.
Pardo-Iguzquiza, E., P. A. Dowd, C. Xu, and J. Jose Duran-Valsero (2012), Stochastic simulation of karst conduit networks, *Adv. Water Resour.*, *35*, 141–150.
Peaceman, D. W. (1983), Interpretations of well-block pressure in numerical reservoir simulation with non-square grid blocks and anisotropic permeability, *Soc. Pet. Eng. J.*, *23*(3), 531–543.
Perne, M., M. Covington, and F. Gabrovsek (2014), Evolution of karst conduit networks in transition from pressurized flow to free-surface flow, *Hydrol. Earth Syst. Sci.*, *18*(11), 4617–4633.
Rehrl, C., S. Birk, and A. B. Klimchouk (2008), Conduit evolution in deep-seated settings: Conceptual and numerical models based on field observations, *Water Resour. Res.*, *44*, W11425, doi:10.1029/2008WR006905.
Reimann, T., C. Rehrl, W. Shoemaker, T. Geyer, and S. Birk (2011), The significance of turbulent flow representation in single-continuum models, *Water Resour. Res.*, *47*, W09503, doi:10.1029/2010WR010133.
Ronayne, M. (2013), Influence of conduit network geometry on solute transport in karst aquifers with a permeable matrix, *Adv. Water Resour.*, *56*, 27–34.
Shoemaker, W. B., E. L. Kuniansky, S. Birk, S. Bauer, and E. D. Swain (2008), Documentation of a Conduit Flow Process (CFP) for MODFLOW-2005, *U.S. Geol. Surv. Tech. Methods*, *Book 6, Chap. A24*, 50 pp.
Siemers, J., and W. Dreybrodt (1998), Early development of karst aquifers on percolation networks of fractures in limestone, *Water Resour. Res.*, *34*(3), 409–419.
Stark, C. P. (1991), An invasion percolation model of drainage network evolution, *Nature*, *352*(6334), 423–425.
Svensson, U., and W. Dreybrodt (1992), Dissolution kinetics of natural calcite minerals in CO_2-water systems approaching calcite equilibrium, *Chem. Geol.*, *100*(1–2), 129–145.
Swamee, P. K., and N. Swamee (2007), Full-range pipe-flow equations, *J. Hydraul. Res.*, *45*(6), 841–843.
Szymczak, P., and A. J. C. Ladd (2009), Wormhole formation in dissolving fractures, *J. Geophys. Res.*, *114*, B06203, doi:10.1029/2008JB006122.
Van Genuchten, M. T. (1980), A closed-form equation for predicting the hydraulic conductivity of saturated soils, *Soil Sci. Soc. Am. J.*, *44*(5), 892–898.
Wang, L., and H. Liu (2006), An efficient method for identifying and filling surface depressions in digital elevation models for hydrologic analysis and modelling, *Int. J. Geogr. Inf. Sci.*, *20*(2), 193–213.
White, W. B. (1977), Role of solution kinetics in the development of karst aquifers, in *Karst Hydrogeology*, edited by J. S. Tolson and F. L. Doyle, pp. 503–517, Int. Assoc. of Hydrogeol., Huntsville, Ala.
Williams, L. J., and J. F. Dixon (2015), Digital surfaces and thicknesses of selected hydrogeologic units of the Floridan aquifer system in Florida and parts of Georgia, Alabama, and South Carolina, *U.S. Geol. Surv. Data Ser.*, *926*, 24 pp.
Xu, C. S., and P. Dowd (2010), A new computer code for discrete fracture network modelling, *Comput. Geosci.*, *36*(3), 292–301.
Xu, Z. X., B. X. Hu, H. Davis, and J. H. Cao (2015), Simulating long term nitrate-N contamination processes in the Woodville Karst Plain using CFPv2 with UMT3D, *J. Hydrol.*, *524*, 72–88.